Solar Driven Interfacial Steam Generation Derived from Biodegradable Luffa Sponge

Ahmed Mortuza Saleque[1a,b], Sainan Ma[1a,2], Safayet Ahmed[1a,b], Mohammad Ismail Hossain[1a,b,3], Wayesh Qarony[4], Yuen Hong Tsang[1a,b,*]

1a.) Department of Applied Physics and Materials Research Center, The Hong Kong Polytechnic University, Hung Hom, Kowloon, Hong Kong

1b.) Shenzhen Research Institute, The Hong Kong Polytechnic University, 518057 Shenzhen, Guangdong, People's Republic of China.

2.) Ningbo Research Institute, Zhejiang University, Ningbo 315100, China

3.) Department of Materials Science and Engineering, City University of Hong Kong, Kowloon, Hong Kong

4.) Department of Electrical and Computer Engineering, University of California, Davis, California, USA

*.) Corresponding author: yuen.tsang@polyu.edu.hk

Abstract:

A chemically treated luffa sponge (LS) derived from the ripe fruit of the Luffa cylindrica (LC) plant was investigated as an efficient solar photothermal conversion material for water purification applications for the very first time. Hydrophilicity and solar absorbance of the LS were enhanced by dopamine treatment and candle soot surface coating. The fabricated surface modified LS (SM-LS) leads to achieving a superb solar evaporation rate of water as high as 1.30 kg m^{-2} h^{-1}, which is 5 times higher than that of the freshwater under 1 sun illumination. The outdoor experiment has shown an excellent solar evaporation efficiency of 79.98%, which is significantly higher than other low-cost materials. Such SM-LS can be further applied to desalinate the seawater, where it has been examined that 1 m^2 of surface-modified LS can produce 7.5–8 L of freshwater per day. Hence, the proposed system can be utilized in remote areas and refugee camps.

1. Introduction

The rising global demand for energy has consistently been considered a peremptory challenge to fulfill human social and economic growth, welfare, and health. Securing energy supply and curbing the contribution of carbon to climate change are the energy sector's two-superseding obstacles on the road to a sustainable future [1–4]. As the proven reserves of fossil fuels decrease, renewable energy sources have been sought in high demand, of which solar power is the most promising and potentially limitless source of

energy in the foreseeable future. The energy from the sun to the earth is as high as 3×10^{24} Jules per year, just 0.1% of the total solar resource would be sufficient to satisfy the annual worldwide energy demand [5–8]. At present, solar-steam generation, which particularly refers to solar vapor under 100 °C, is considered to be one of the most promising sectors among other solar energy harvesting technologies owing to its potential applications in modern power plants, chemical plants, liquid-liquid phase separation, water purification and desalination, wastewater treatment and many others [5,9–16]. Among which water purification and desalination are gaining a lot of interest due to the recent lack of drinkable clean water supplies across the globe. Other competitive technologies for the production of freshwater, such as solid-liquid extraction [15,17], electrochemical analysis [18,19] membrane-based separation [20,21], etc. have many drawbacks, including high energy usage, possible environmental emissions, high infrastructure capital costs, etc.

However, the efficiency of the traditional solar-steam generation method is below 24%, even with a high optical concentration ratio [22]. The traditional approach involves water evaporation by converting solar radiation directly to heat for steam generation commonly by using bulk metals. These bulk metals are inefficient in absorbing the solar spectrum and transferring heat through bulk water. As a consequence, its performance is limited by localized heat generation and transfer losses [14,23,24]. By contrast, interfacial solar vapor generation (ISVG) can localize the heat on the evaporation surface and, rather than the whole water, selectively heat the evaporation portion to minimize heat transfer to the water and significantly increase the solar evaporation efficiency. Therefore, ISVG has emerged as a novel concept for the solar steam generation with higher efficiency,

attributes to the recent developments in nano-scale structural design with efficient photon and thermal management known as photothermal conversion materials [8,25–29]. The photothermal conversion materials should have strong solar absorption and low thermal conductivity to achieve greater efficiency [7,14]. Moreover, it is also desirable to have superior hydrophilicity and porosity for fast water and steam transport [30–32]. Therefore, the design of photothermal conversion material is a pivotal challenge to realize the sustainable and practical application of solar steam generation.

Recent research on generating solar steam has focused primarily on exploring photothermal materials with high absorption in the solar spectrum. Many researchers have investigated plasmonic absorbers [33] and noble metallic and non-metallic nanoparticles such as NiO nanoparticles [34], MoS_2 nanosheets [35–38], processed wood [39–41], activated carbon [42,43], carbon nanotube [44–46], carbon black [47–49], carbon foam [47,49–51], carbon fiber [52–54], graphene and graphene oxide [43,55–57], Au nanoparticles [58–62] on finding efficient photothermal conversion materials for the top layer to absorb the incident solar irradiation and convert it into heat energy. Many research groups [63–66] demonstrated the use of 3D porous graphene/carbon hybrid aerogels as photothermal material and achieved significantly higher photothermal efficiency under 1 sun (1 sun = 1 kW m^{-2}) illumination. Nevertheless, these recorded materials, films, and floating particles are either expensive or toxic and, therefore, not suitable for large-scale production of drinking water. Therefore, the use of low-cost materials for ISVG has drawn a great interest among the researchers. S. Ma et al. [7] and H. Cheng et al. [67] reported that chemically treated polyurethane sponges to develop a solar water purification system. But polyurethane foam is not undoubtedly safe to produce drinking water as it contains

isocyanates [68], which is widely known as respiratory toxin [69]. The use of treated wood has been explored in many studies intending to produce steam at a significantly lower cost. M.M. Ghafurian et al. [70] demonstrated the laser carbonization and gold nanolayer deposited wood for the generation of water steam at a comparable cost to synthetically processed wood for the same purpose. But this configuration showed satisfactory evaporation rate at 3 sun illumination, thus hindering the scalable application under natural condition. Other researchers [70–74] investigated an alternative approach for using processed wood as photothermal conversion material. Nonetheless, these methods require a variety of complicated preparation steps involving costly and toxic chemicals. Therefore, we plan to use naturally available low-cost non-toxic material, which can be used as photothermal conversion material after a few simple chemical processing steps to generate solar steam sufficient performance. The feasibility of the practical implementation to produce drinking water is also a vital concern of this research.

Luffa sponge, also known as sponge gourd, is a commercially available and biodegradable substance with a fibrous vascular reticulated structure derived from the ripe fruit of *Luffa cylindrica* (LC) plant. This subtropical plant is abundant in Asia, central and southern America. The fibrous network structure of luffa sponge serves like open-cell foam material, thus allowing it to float on the water surface [75,76]. It is relatively stable in its intended lifetime and has the potential to be used as an alternative material for man-made cellular materials. Though it has moderate hydrophilicity property, the hydrophilicity can be further increased by chemical treatment [76]. Also, there are a large number of microcracks on the surface of luffa fibers that can collect and store water by capillary mechanisms [77], thus reveals its potential to be used as solar photothermal conversion

material. Previously, luffa sponge has been successfully used in many applications such as bio-fibers manufacturing [78], bio-sorbent to the removal of divalent metals, oil absorption, CO_2 chemical fixation [79], efficient phenol degradation [77], composite materials [80] and also in Li-ion batteries [81,82]. To the best of our knowledge, no application of candle soot coated luffa sponge as the material for solar photothermal conversion has been demonstrated till now.

In this work, for the first time, we report the use of chemically treated luffa sponge with candle soot coating on the top surface as solar photothermal conversion material for steam generation. Its porous structure, self-floating properties, biodegradability, easy availability, environmental sustainability, flexibility, ease of processing, and impressive physio-mechanical properties [83] make it the ideal candidate for solar absorber with the exception of its moderate hydrophilicity. Dopamine solution treatment was employed to alter the surface chemical properties to improve the hydrophilicity of the luffa sponge. The black candle soot coating on the top surface of the dopamine treated luffa sponge enhanced the solar absorption. Candle soot is a well-known cost-effective source of carbon nanoparticles and exhibits superb solar absorbent property [84,85]. The dopamine treated luffa sponge with the black candle soot coating on the top surface as referred by surface-modified luffa sponge (SM-LS) in this paper, achieved 64.75% evaporation efficiency under one sun illumination while taking into account the spontaneous evaporation in the dark field and 3.8 times higher evaporation rate compared to pristine luffa sponge. A small prototype was developed to demonstrate the performance of SM-LS in outdoor clean water production. During the outdoor experiment on a sunny day, close to 80% efficiency was achieved using the custom-made prototype. This remarkable

solar evaporation efficiency is owing to the superior solar absorption due to the candle soot coating and natural capillary mechanism, high porosity & increased hydrophilicity of the dopamine treated luffa sponge. Also, it preserved stable evaporation levels for roughly 21 wetting-drying applications for various water purification and thus displayed outstanding recycling reliability. The ohmic resistance method and inductively coupled plasma mass spectroscopy based ion analysis method was used to demonstrate the effectiveness of SM-LS in desalination and purification of polluted water. It was found that 1 m^2 SM-LS (cost $ 4.5 per m^2) was capable of generating 7.5−8 liters of freshwater per day on a typical sunny day in Hong Kong during summer. Cycling ability, field experiment results and superior desalination/purification efficiency compare to other biodegradable materials such as plasmonic wood [86], flame-treated wood [87], carbonized bamboo [88] etc. demonstrate the effectiveness of SM- LS for practical and efficient water purification.
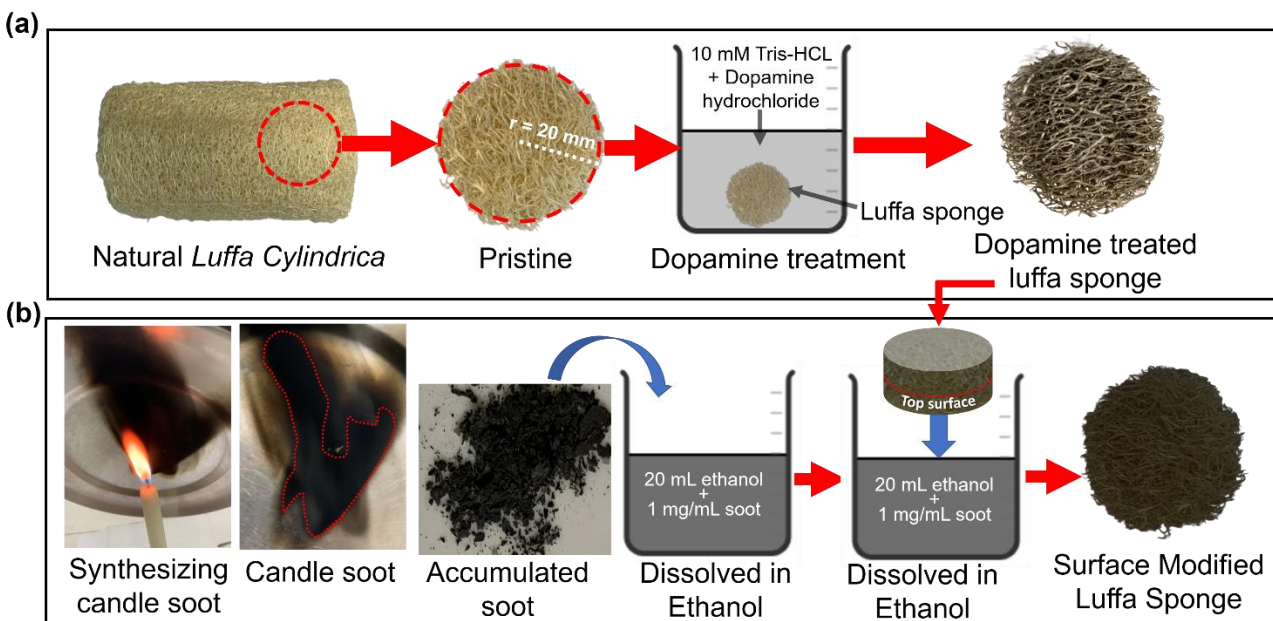
Figure 1. Schematic diagram of surface-modified luffa sponge (SM-LS) preparation process: (a) preparation of hydrophilic dopamine treated luffa sponge; (b) Candle soot accumulation and coating on the top surface of the dopamine treated luffa sponge

2. Material and methods

2.1 Materials

The pristine luffa sponge was purchased from Hydrea London that came into a cylindrical shape with a diameter of 5.8 cm and 18 cm in length. Its lignocellulosic material composed mainly of 65.5% cellulose, 17.5% hemicellulose and 15.2% lignin [89]. Dopamine hydrochloride (98%), Tris (hydroxymethyl) aminomethane hydrochloride (Tris-HCl) (pH 8.8, 1.5 M), and ethanol (C_2H_5OH > 99%) were provided by J & K Scientific Ltd. (Beijing, China). All the chemicals were used as received without further purification.

2.2 Preparation of hydrophilic luffa sponge

The cylindrical form of luffa sponge was halved, and a sharp scissor was used to carefully extract the central fibrous vascular structure. It was then tailored to a circular shape with a diameter of 40 mm and a thickness of 12 mm as shown in **Figure 1a**. The sample was then ultrasonically washed for three times with distilled water (DI) and ethanol, followed by drying in an oven at 55 ° C. The dopamine solution (2 mg ml^{-1}, pH = 8.8) was obtained by dissolving dopamine hydrochloride in 10 mM Tris-HCl. The washed sponge luffa (LS) sample was soaked into 20 ml of freshly prepared dopamine solution, then stirred overnight. The as-prepared SM-LS sponge was then washed with DI water several times and dried in the oven at 55 ° C for 4 h.

2.3 Candle soot coating on the top surface of treated luffa sponge

A stainless-steel plate and paraffin wax candle were used to synthesize candle soot. The stainless-steel plate was washed several times using absolute ethanol. After that, the dried stainless-steel was placed in the middle position of a candle flame for 5 mins. The soot layer was deposited in the stainless-steel as shown in **Figure 1b**, which can be

scraped off the stainless-steel plate. The cycle has been repeated several times to produce enough amount of candle soot in a crucible. The accumulated soot was treated at 100 ° C for 2 h atmospheric to remove the unburned wax coating. 1 mg mL^{-1} concentration of candle soot was dissolved into 20 mL of ethanol ($C_2H_5OH > 99\%$) and stirred overnight. Since the top surface of the dopamine treated luffa sponge needs to be coated with candle soot, only the top surface (5 mm in thickness) was carefully dipped into the solution for an hour in an upside-down position. Then the sample was dried at room temperature overnight, keeping in the upside-down position. The method of coating is illustrated in **Figure 1b**.

2.4 Materials characterization

The morphologies of the pristine and SM-LS were characterized using scanning electron microscopy (SEM; TESCAN, VEGA3) with an acceleration voltage of 20 kV. An attenuated total reflection Fourier transform infrared spectroscopy (ATR-FTIR) was obtained by a VERTEX 70v spectrometer (Bruker, Karlsruhe, Germany). The spectra were obtained over a range between 400 and 4000 cm^{-1} with a spectral resolution of 4 cm^{-1}. The UV-VIS-NIR spectrum was achieved by PerkinElmer Lambda 1050 UV-VIS-NIR spectrometer. The Ohmic resistance of purified water was measured by using a multimeter (ProsKit MT-1217).

2.5 Experimental setup for solar steam generation

Both indoor and outdoor experiments were conducted to assess the performance of the SM-LF. The indoor steam generation experiment was conducted by floating the pristine and surface modified luffa sponge in a quartz beaker. The samples are 40 mm in diameter and 12 mm in thickness. The weight losses due to the water evaporation were measured

under various irradiation intensities ranging from 1 to 5 kW m^{-2} by a 300 W xenon lamp (PLS-SXE300, Beijing Perfect Light Technology Co., Ltd) and the data were collected by an electronic microbalance (Ohaus Corporation, CP213) with a deviation of 0.1 mg. The solar irradiation intensity at the surface of the sample was measured by a power meter (THORLABS, S314C). An infrared (IR) camera (FLIR-E64501, Tallinn, Estonia, error range of ± 2 °C) was used to monitor the change in temperatures. All the indoor experiments were conducted in a laboratory environment at room temperature of 20 ± 1 °C and humidity of about 60%. The outdoor experiment was conducted at an open sky garden in Hung Hom, Hong Kong under the clear sky. A sample of 50 mm in diameter and 12 mm in the thickness of pristine luffa sponge was chemically treated to convert to SM-LF. This new sample was put in a custom-made prototype to conduct the experiments with replicated seawater and pullulated river water which is described more details in section 3.5.
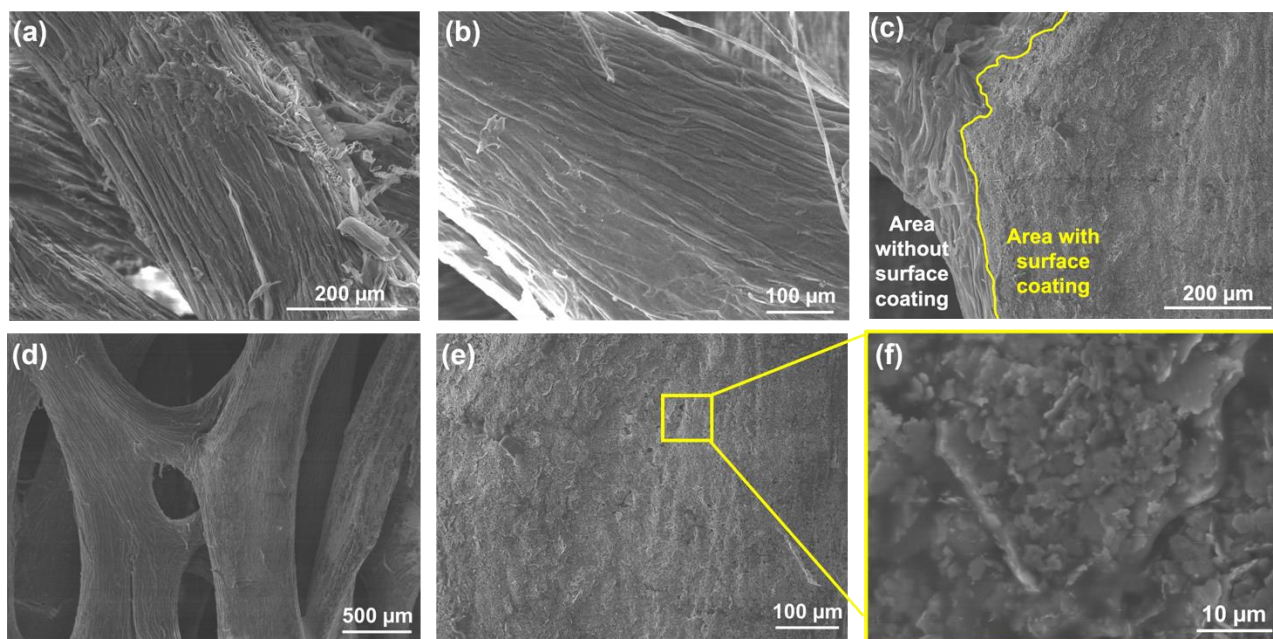
Figure 2. (a) and (b) SEM images of pristine luffa sponge at different magnifications; (c) to illustrate the difference, a portion of the dopamine-treated luffa sponge was coated with

candle soot and other portion remained uncoated; (d-f) SEM images of SM-LS at different magnifications.

3. Results and discussion

3.1 Material structure and morphology

Since the hydrophilicity of the pristine luffa sponge is not good enough, dopamine treatment is used to spontaneously polymerize it into polydopamine (PDA) with a significant number of phenolic hydroxyl groups and deposited on the surface of the luffa sponge [7,90]. Therefore, this chemical treatment process not only serves to increase the wettability of the luffa sponge but also to change the color to black as depicted in Fig. S1a and b (supplementary information). The SEM images in **Figure 2** reveals that the SM-LF has a smoother surface than the pristine luffa sponge. The smoother surface of the SM-LS provides less light scattering than the pristine luffa sponge, resulting in an increase in absorption of the solar spectrum. From the **Figure 2e**, it can be observed that the candle soot are deposited uniformly over the surface area. In order to have a better understanding of surface coating, a portion of a dopamine treated luffa sponge was coated with candle soot while the other portion remined uncoated. In the SEM image as shown in **Figure 2c**, a clear distinction between the coated and uncoated surface area can be observed very nicely. In addition, the surface wetting property of the SM-LS was characterized by water contact angle measurement. The water contact angle has been decreased from 119.36° to 66.48° after applying the candle soot coating on the dopamine treated luffa surface as represented in **Figure 3d and e**. This reduced water contact angle results in an increased hydrophilicity property which is beneficial for the heat localization and the transfer of water, thereby promoting the process of solar evaporation.

As shown in **Figure 3**, unlike the FTIR spectrum of the pristine luffa sponge, the dopamine treated luffa sponge (before applying the candle soot coating) FTIR spectrum has a significant absorption band at 3250 nm arising from O—H stretching; the 2040 nm band is due to the stretching vibrations of C==O, and the band at 1023 nm band can be related to the C — O stretching band [6]. A good number of O—H and C===O groups indicate the excellent hydrophilicity of the SM-LS [91]. The intrincis optical absorption property of the pristine luffa sponge and the SM-LS was determined by UV-VIS-NIR spectrometer. As shown in **Figure 3c**, the overall absorption was significantly increased after the dopamine treatment and surface coating. The SM-LS was found to have higher absorbance (over 90%) in the near-infrared region (780-2500 nm). However, the absorbance in the ultraviolet and visible regions (300-780 nm) was about 80%. This increased absorbance of SM-LS help to obtain higher evaporation rate. In addition , the lower vascular structure density of the luffa sponge (15 kg m^{-2}) allows it float on the water surface. The enhanced vaoupr generated under the 5 kW m^{-2} solar illumination by the SM-LS can be easily observed in **Figure 3f**.
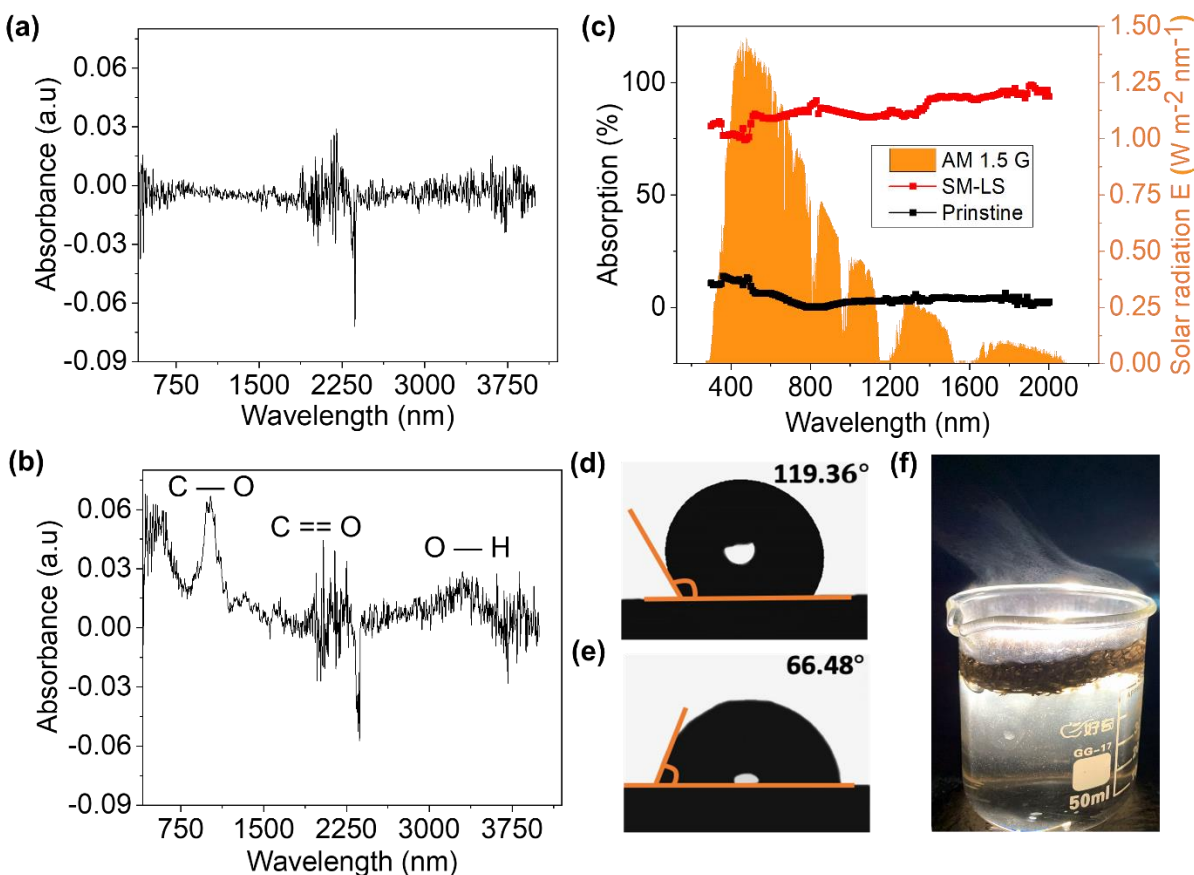
Figure 3. ATR-FTIR spectra of (a) Pristine luffa sponge; (b) Dopamine treated luffa sponge; (c) UV-VIS-NIR absorption spectrum of pristine and SM-LS. Contact angle measurement of (d) Pristine luffa sponge and (e) SM-LS. (f) Enhanced vapor generation by SM-LS at 5 kW m^{-2} solar illumination.

3.2 Evaluation of the solar evaporation by SM-LF

Solar evaporation tests were performed for an hour in a laboratory setting using a beaker, pristine luffa sponge, SM-LF, and xenon lamp simulated as solar light source, as shown in **Figure 4a** and **Figure S2**. Experiments were conducted to measure the evaporation rate of freshwater, pristine luffa sponge, and SM-LF under one sun illumination by measuring the mass loss as a function of time, respectively. The computer-controlled electronic balance system recorded the mass loss data at every 10-sec intervals. The spontaneous evaporation of water at dark conditions was measured as 0.187 kg m^{-2} h^{-1}.

The evaporation rates of freshwater and pristine luffa sponge were recorded as 0.26 kg m^{-2} h^{-1} and 0.35 kg m^{-2} h^{-1} respectively under the same laboratory condition (temperature 20 ± 1 °C and humidity 60%). On the contrary, the water evaporation rate was enormously enhanced after using SM-LS. As can be seen in **Figure 5a**, the SM-LS water evaporation rate is 1.3 kg m^{-2} h^{-1}, which is 5 times greater than that of the pure water only without luffa sponge, thereby demonstrating the outstanding potential of SM-LS to accelerate the generation of solar steam. The obtained evaporation rate for SM-LS is higher than that of most of the materials reported to date, which is represented in **Table 1**.

The evaporation efficiency, $\eta_{solar\text{-}ev}$, can be expressed by the following formula.

$$\eta_{solar-ev} = \frac{\dot{m}h_{LV}}{A\,q_{solar}} \qquad (1)$$

where $\dot{m}$ is the evaporation rate (kg m^{-2} h^{-1}), A is the efficient absorber area (m^2), q_{solar} is the incident solar flux per unit area (kW m^{-2}) and h_{LV} is the phase change enthalpy of water (kJ kg^{-2}), which can be expressed as the summation of sensible heat and latent heat during the steady-state solar steam generation process.

$$h_{LV} = C.\Delta T + h_{vap} \qquad (2)$$

where C is the specific heat capacity of water (4182 J kg^{-1} K^{-1}), ΔT is the increase in water temperature (K), and h_{vap} is the latent heat of vaporization at steady-state condition (kJ.kg^{-1}).

Figure 4. Schematic diagram for the evaluation of the solar evaporation: (a) laboratory setup; (b) setup for the practical experiments
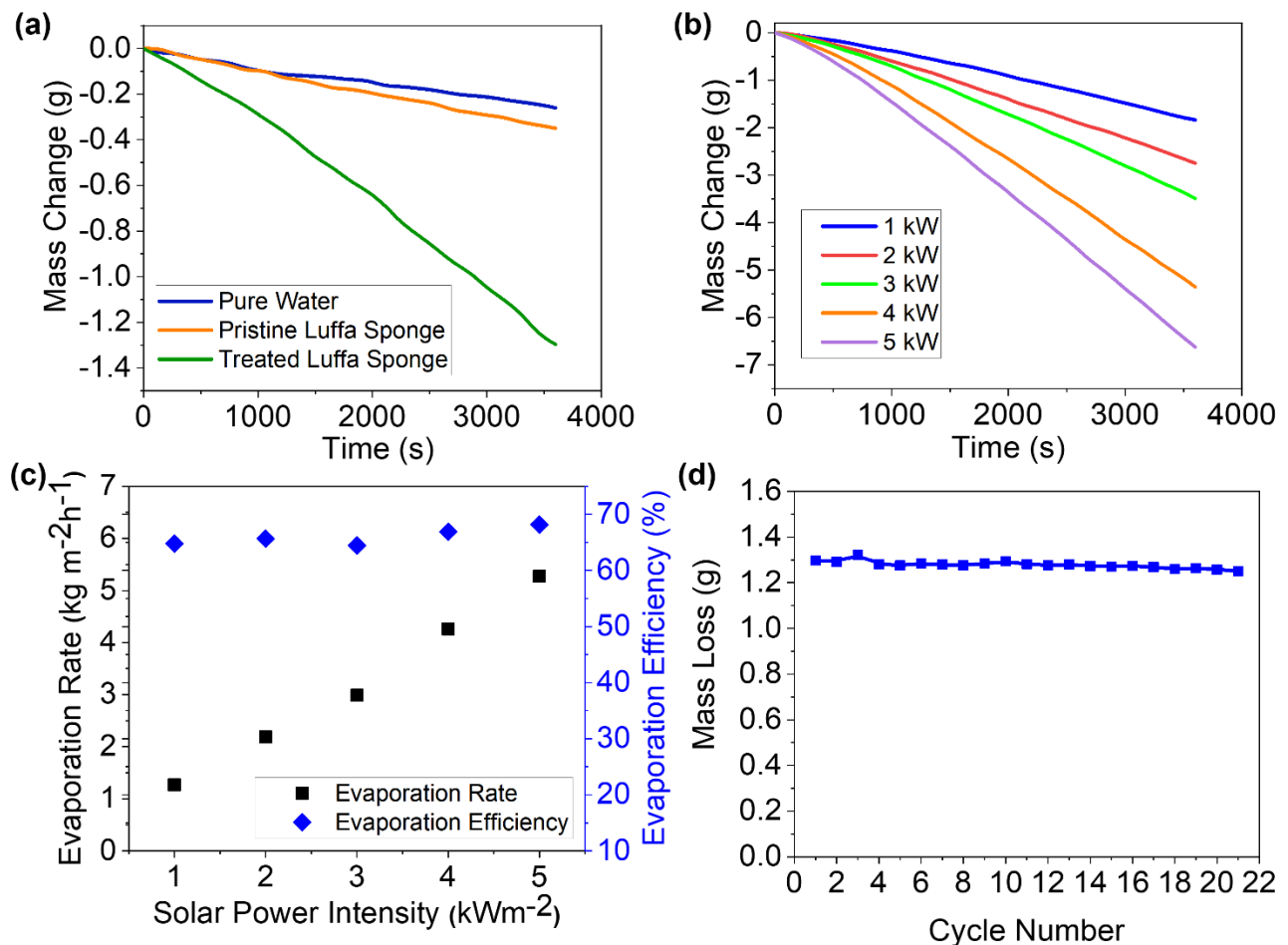
Figure 5. The solar evaporation mass loss of water over time (a) with different absorbers under one sun illumination; (b) with SM-LS under various solar irradiance; (c) corresponding evaporation rate (square) and the evaporation efficiency (star) under various solar irradiance; (d) mass loss using SM-LS for 21 cycles (each cycle corresponds to 1 h under 1 kW m^{-2} irradiance)

The contribution of dark evaporation should be subtracted to calculate the net solar-driven evaporation output. Hence equation (1) can be rewritten as

$$\eta_{solar-ev} = \frac{\dot{m}h_{LV}|_{solar} - \dot{m}h_{LV}|_{dark}}{A\,q_{solar}}$$ (3)

Here $\dot{m}_{dark}$ is the evaporation rate in the dark (kg m^{-2} h^{-1}).

Under one sun illumination, the evaporation efficiency of SM-LS was calculated as 64.79%, which is 5 times higher than the average evaporation efficiency of the freshwater of 14.5%. **Figure 5b** depicts the mass loss of SM-LS at various solar illuminations. The mass loss significantly increases at higher solar intensities. **Figure 5c** indicates the evaporation rate at various solar illuminations. The average evaporation rate was 1.27 kg m^{-2} h^{-1} under 1 sun illumination and reached 5.27 kg m^{-2} h^{-1} as the solar illumination level increased to 5 kW m^{-2}.

Figure 5c also reveals that the evaporation efficiency becomes maximum when the solar illumination is set at 5 kW m^{-2}. However, under 1 sun illumination, the evaporation efficiency is still as high as 64.79%. Over the wide range of variations in solar illumination, the evaporation efficiency fluctuation was very low, with a margin of < 3.5%. Furthermore, the cycling efficiency of SM-LS has been investigated. After every solar evaporation experiment, SM-LS was dried in the oven at 55 ° C for 1 hour. As seen in **Figure 5d**, after 21 times wetting-drying cycles, SM-LS still provides solar evaporation mass losses of more than 1.25 kg m^{-2} h^{-1} for freshwater, showing the excellent cycling stability of SM-LS for steam production. Each experiment was repeated four times under the same experimental conditions. The standard deviation was calculated based on the average data which is further explained in supplementary information. The discrepancy between the measurements is less than 4%, showing the reproducibility of the experimental

results. The error is primarily attributed to variations of room temperature, humidity, and precision of the instrument. Two separate one-hour tests data is also provided in supplementary information.

Table 1 Performance comparison

Used material	Evaporation rate under 1 sun $(kg\ m^{-2}\ h^{-1})$	Maximum Evaporation Efficiency	References
RVC foam	-	25%	[92]
Black polyurethane	0.83	52.2%	[7]
Carbonized bamboo	1.547	62.3%	[88]
Carbonized facial tissue	-	64%	[93]
Foam with bubble wrap	-	64%	[8]
Carbonized nanotube modified flexible wood	0.95	65%	[94]
Plasmonic wood	-	68%	[86]
Flame-treated wood	1.05	72%	[87]
Polyvinyl alcohol sponge coated with charcoal	1.02	73%	[95]
Modified NiO disc	1.13	73%	[35]
Carbonized wood with holes	1.04	75%	[91]
Activated carbon	1.22	79.4%	[43]
Surface Modified Luffa Sponge with candle soot coating	1.30	79.98%	This work

3.3 Heat Loss equations

The convective heat transfer loss $q_{convection}$ can be calculated according to Newton's law of cooling.

$$q_{convection} = Ah(t_s - t_a) \tag{4}$$

Here h is defined as the convective heat transfer coefficient of air in natural convection, selected as 5 W m^{-2} K^{-1} [25,26,92,96]. t_s and t_a are the temperature of the top surface and ambient temperature, respectively. Therefore, the ratio of the energy losses caused by the convective heat transfer can be calculated by the following equation.

$$\eta_{convection} = \frac{Ah(t_s - t_a)}{Aq_{solar}} = \frac{h(t_s - t_a)}{q_{solar}} \tag{5}$$

The $\eta_{convection}$ is calculated to be 8.1% under one sun irradiance.

The energy losses due to the thermal radiation from the top surface of the SM-LS can be calculated by using the Stefan-Boltzmann equation.

$$q_{radiation} = \varepsilon A\sigma(t_s{}^4 - t_a{}^4) \tag{6}$$

where σ is the Stefan-Boltzmann constant (5.67×10^{-8} W m^{-2} K^{-4}), and ε is the emissivity of the surface. For the SM-LS the calculated emissivity is about 0.97 (details equations are provided in supplementary information). The radiation loss rate can be expressed by,

$$\eta_{radiation} = \frac{\varepsilon A\sigma(t_s{}^4 - t_a{}^4)}{Aq_{solar}} = \frac{\varepsilon\sigma(t_s{}^4 - t_a{}^4)}{q_{solar}} \tag{7}$$

The value of $\eta_{radiation}$ is calculated as 9.75%.

The energy loss due to the heat conduction from the bottom layer of the SM-LS to the water can be calculated by using the temperature gradient and Fourier's law,

$$q_{conduction} = kA\frac{\Delta T}{L} \tag{8}$$

where k = 0.617 W m^{-1} K^{-1} which is known as the thermal conductivity of water. The temperature gradient $\left(\frac{\Delta T}{L}\right)$ is 180 K m^{-1} under one sun illumination as the temperature measured at the bottom surface of the SM-LS and 2 cm down to the bottom surface were

36.2 and 32.6 °C, respectively. The percentage of conductive heat loss can, therefore, be determined by,

$$\eta_{conduction} = \frac{kA^{\Delta T}/_L}{Aq_{solar}} = \frac{k^{\Delta T}/_L}{q_{solar}} \qquad (9)$$

Thus, the calculated $\eta_{conduction}$ accounts for 11.11%. The ISVG process is reckoned as a dynamic equilibrium of different energy flows, which reads:

$$\eta_{solar} = \eta_{convection} + \eta_{radiation} + \eta_{conduction} + \eta_{evaporation} \qquad (10)$$

$\eta_{evaporation}$ is the efficiency of the energy transferred for water evaporation which can be calculated as 71.04% from equation (10). However, the efficiency of evaporation under one sun is estimated at 64.79% with equation (1). The evaporation efficiency difference of 6.25% can be realized as a result of reflection loss. Nevertheless, the heat losses can be tapered into lower values in real-life applications where the enclosed device is designed. An electrical equivalent heat transfer model is presented in supplementary information.

3.4 Mechanisms of solar steam generation enhancement

To achieve higher evaporation efficiency, a localized heat zone at the air-water interface is necessary. At the same time, the loss of heat transfer from the localized heat zone should be limited to improve steam generation. The significantly lower thermal conductivity of luffa sponge [97,98] allows retaining localized surface heat. Besides, the dopamine treatment of the luffa sponge trends to enhance its hydrophilicity, enabling the water molecules to migrate through the localized heat zone. The increment of the evaporation process using the localized heat can be calculated by applying Dalton's law of potential evaporation rate as expressed in equation (11).

$$E = \frac{\rho T_{air} GW(P_s - P_{air})}{P} \qquad (11)$$

Where, E is the evaporation rate, ρ is the air density (kg m^{-3}), T_{air} is the air temperature

(°C), G is the conductivity to steam from evaporating surface (m/day), W is the wind speed

in the direction of the tangent to evaporation surface (m s^{-1}), P is the air pressure (P$_a$) and

P_s and P_{air} are the saturation and realistic vapor pressure of the liquid respectively. As

the saturation vapor pressure increases with the temperature rise, the evaporation rate

depends on the surface temperature. The infrared (IR) camera was used to measure the

temperature distribution at the surface and the underlying bulk water. As seen from the

Figure 6, the temperature was uniformly distributed to the top surface and underlying

bulk water of both beakers with and without SM-LS at about 20.5 °C before irradiation.

But after applying 1 kW m^{-2} solar irradiance for one hour, the surface temperature of the

beaker without SM-LS was raised by 8 °C as depicted in **Figure 6a**. The temperature

difference between surface and underlying bulk water was only 1.9 °C which implies that

the temperature distribution was nearly uniform. In contrast, under the same experimental

condition, the surface temperature of the beaker with SM-LS was increased to 36.2 °C,

and the temperature difference between the surface and the underlying bulk water was

14.1 °C as shown in **Figure 6b**, thus confirming the existence of a localized heat zone on

the air-water interface. The water transported to the top surface of the SM-LS through the

pores channel of the luffa sponge and then converted into steam. In addition, the average

cost of fabricating 1 m^2 of SM-LS was calculated to be $ 4.5 for the small laborary scale

production. In brief, the excellent efficiency of solar evaporation, the remarkable cycling

ability, and the cost-effective processing of SM-LS are favorable for practical application.
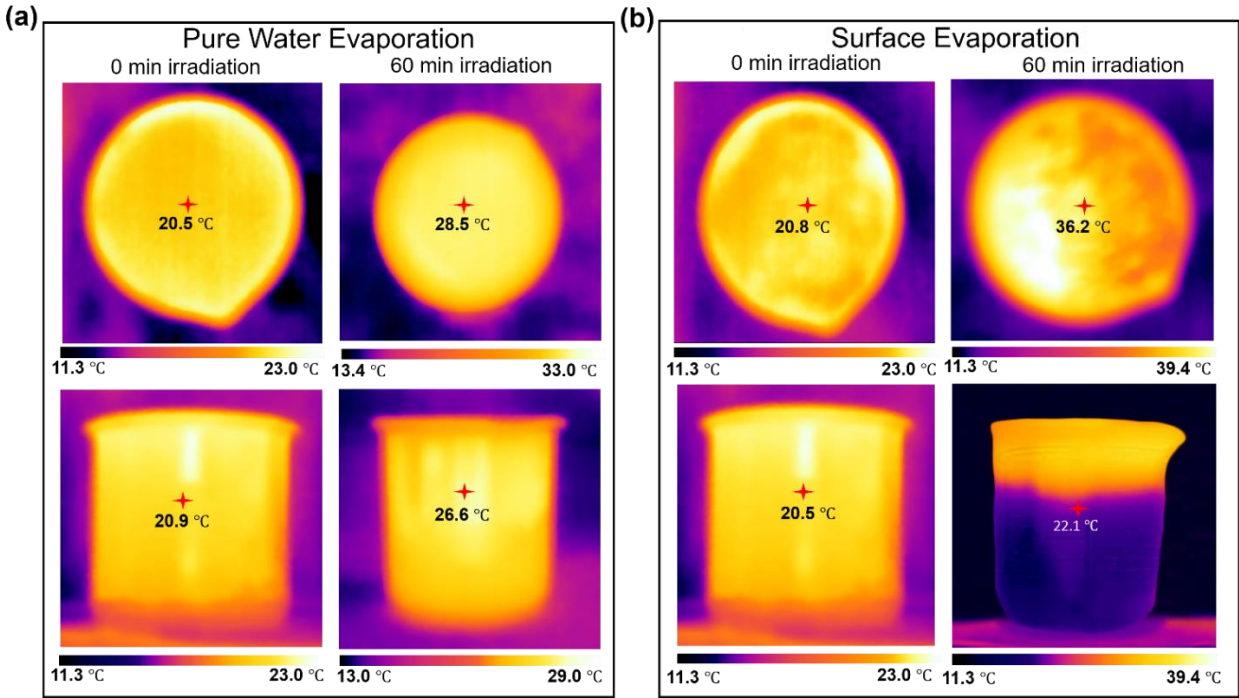
Figure 6. Top view and side view IR camera images of (a) freshwater evaporation at 0 min and 60 min irradiation under one sun illumination; (b) surface evaporation with SM-LS at 0 min and 60 min irradiation under one sun illumination.

3.5 Potential application: seawater desalination and polluted water purification

The objective of developing the SM-LS is to extend it to the realistic application of desalination and purification of water. As a result, outdoor experiments were conducted on a sunny day to demonstrate solar desalination and purification performance using a custom-made setup as shown in **Figure 7g**. Seawater is replicated by dissolving 6.68 g of NaCl, 0.05 g of $NaHCO_3$, 0.87 g of Na_sSO_4, 0.18 g of KCl, 0.57 g of $MgCl_2$, 0.81 g of $MgSO_4$, and 0.28 g of $CaCl_2$ in 250 mL of DI water [99]. Polluted water was collected from the Turag river situated in Tongi, Dhaka, Bangladesh. As shown in **Figure 7g**, the enclosed structure made by transparent glass contained the water sample.
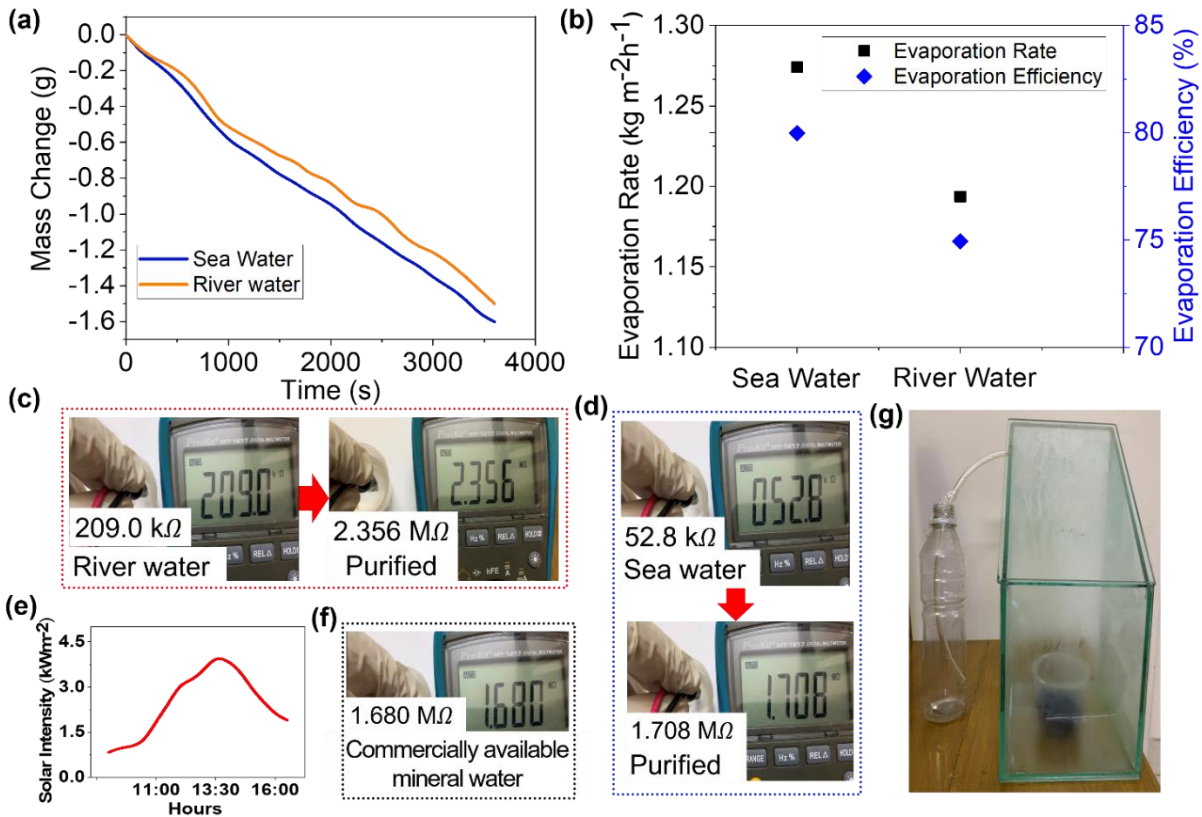
Figure 7. Demonstration of the outdoor performance of the SM-LS purifying sea and river water (a) mass change; (b) evaporation rate and efficiency; (c), (d) and (f) resistance of river water, replicated seawater, commercially available minarel water respectively; (e) measured solar intensity during the outdoor experiment; (f) water desalination and purification prototype.

This prototype was placed at an open sky garden in Hung Hom, Hong Kong under the clear sky from 9:00 a.m. to 4:30 p.m. for the experiments. The solar irradiance was also measured by the power meter (THORLABS, S314C). A portion of the generated steam was condensed at the top plate which is placed at a sloping angle thus enabling us to collect the water droplet from the bottom of the prototype. Rest of the steam was collected through a hole at the top of the prototype. A plastic pipe was used to gather the steam inside a plastic bottle connected to the other end of the connecting pipe, serving as a condenser. The steam radiates its temperature and turns into a water droplet at a faster

rate. The freshwater production rate as shown in **Figure 7a** was determined to be 1.601 and 1.50 kg m^{-2} h^{-1} for the seawater and polluted river water, respectively, resulting in an evaporation efficiency close to 80% as indicated in **Figure 7b**.

The desalination and purification performance of the SM-LS was determined by measuring electrical resistance, ion concentrations and salinity. The replicated seawater and polluted river water had a very low resistance in comparison to desalinated and purified water. As depicted in **Figure 7c and d**, the purified water consensed from river water and seawater had higher resistance 2.356 and 1.708 MΩ respectively, which is 38 times higher than that of seawater (58.7 kΩ, **Figure 7d**) and 11 times higher than river water (0.2 MΩ, **Figure 7c**). Whereas the resistance of commercially available mineral bottled water is 1.68 MΩ thus indicating the excellent water purification capability of SM-LS. To further access the performance of the SM-LS, inductively coupled plasma mass spectroscopy was used to measure the presence of the ions (Na^+, K^+, Ca^{2+}, Mg^{2+}) in the desalinated water as condensed during the solar evaporation. As depicted in **Figure 8a and b**, ion concentrations and salinity were drastically reduced relative to replicated seawater and were well below the maximum amount of ions approved in drinking water as set by the World Health Organization (WHO) [100,101] . Therefore, SM-LS can be efficiently used desalination and water purification applilcation.

Furthermore, considering that 5 h is the average solar day, 7.5 to 8 liters of freshwater can be produced from 1 m^2 of SM-LS on a typical sunny day in South-East Asia. Whereas adult men need only 3.7 liters of drinking water as determined by the World Health Organization [101].
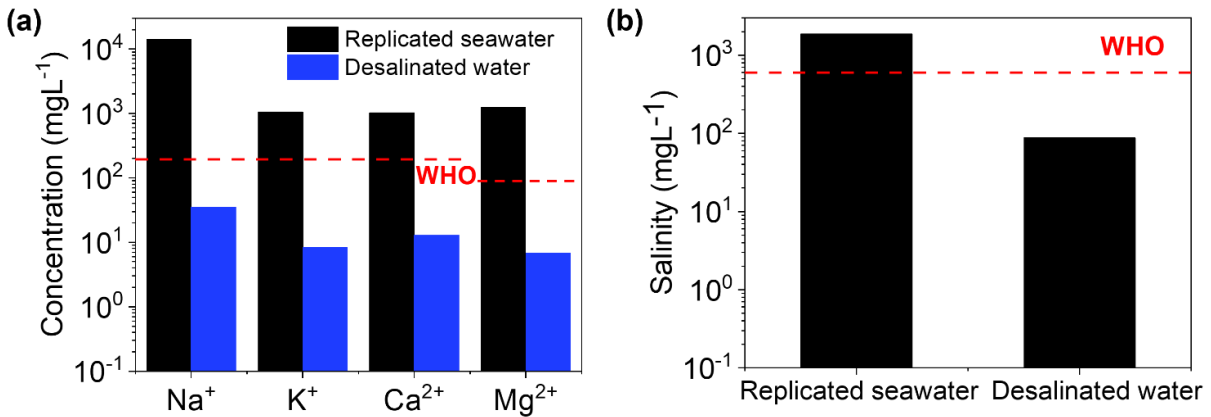
Figure 8. (a) Concentration of ions and (b) Salinity in replicated seawater and desalinated water. The dashed line demoted the World Health Organization (WHO) standard of ions and salinity for drinking water.

As a result, an area of ~2.5 m^2 on the rooftop is required to produce 18.50 liters of purified drinking water per day, which is sufficient for 5 adults of a typical cluster family. In addition, this prototype can be a cost-effective solution for generating fresh drinking water in remote locations as well as in refugee camps located in different parts of the world. The usage of SM-LS as a solar absorber material, therefore, shows exciting prospects for realistic applications.

4. Conclusion

In this paper, we have successfully demonstrated the use of biodegradable eco-friendly luffa sponge and candle soot as a solar absorber for the construction of an interfacial solar vapor generation system. Besides low cost and biodegradability, one of the key advantages of this design lies in its simple fabrication process, which can be conveniently carried out in any laboratory without the use of sophisticated equipment. Dopamine treatment of the luffa sponge increased its hydrophilicity property, thereby helping to carry the underlying water to its top surface. As the top layer of the dopamine treated luffa

sponge was coated with the candle soot, which is one of the cheapest sources of carbon nanoparticles, the absorption of the solar spectrum increases. The lower thermal conductivity offered by the luffa sponge, therefore, helps to create a localized heat zone at the air-water interface. More significantly, the fabricated SM-LS offers a considerably higher efficiency of 64.79% and a remarkable evaporation rate of 1.30 kg m^{-2} h^{-1}, which is 5 times greater than that of the freshwater under one sun illumination. Additionally, the field test with a prototype made of transparent glass demonstrated the outstanding performance with the efficiency of 79.98% for the SM-LS in desalination application. The recyclability, higher efficiency, and superb evaporation rate make it possible to produce 7.5-8 liters of freshwater using 1 m^2 of SM-LS on a typical sunny day. Since the design involves widely available and very low-cost materials, this prototype can be implemented in refugee camps to meet the drinking water demand.

Conflict of interest statement

The authors declare no conflict of interest.

Reference:

[1]   M. Gholikhani, H. Roshani, S. Dessouky, A. T. Papagiannakis, *Appl. Energy* **2020**, *261*, 114388.

[2]   M. Gholikhani, H. Roshani, S. Dessouky, A. T. Papagiannakis, *Appl. Energy* **2020**, *261*, 114388.

[3]   J. A. Andrés-Mañas, L. Roca, A. Ruiz-Aguirre, F. G. Acién, J. D. Gil, G. Zaragoza, *Appl. Energy* **2020**, *258*, 114068.

[4]   P. A. Owusu, S. Asumadu-Sarkodie, *Cogent Eng.* **2016**, *3*, DOI 10.1080/23311916.2016.1167990.

[5]   L. Zhou, X. Li, G. W. Ni, S. Zhu, J. Zhu, *Natl. Sci. Rev.* **2019**, *6*, 562.

[6]   G. Xue, Q. Chen, S. Lin, J. Duan, P. Yang, K. Liu, J. Li, J. Zhou, *Glob. Challenges* **2018**, *2*, 1800001.

[7]   S. Ma, C. P. Chiu, Y. Zhu, C. Y. Tang, H. Long, W. Qarony, X. Zhao, X. Zhang, W. H. Lo, Y. H. Tsang, *Appl. Energy* **2017**, *206*, 63.

[8]   M. Gholikhani, H. Roshani, S. Dessouky, A. T. Papagiannakis, *Appl. Energy* **2020**, *261*, 114388.

[9]   J. Li, X. Zhou, J. Zhang, C. Liu, F. Wang, Y. Zhao, H. Sun, Z. Zhu, W. Liang, A. Li, *ACS Appl. Energy Mater.* **2020**, *3*, 3024.

[10]   O. Neumann, A. D. Neumann, S. Tian, C. Thibodeaux, S. Shubhankar, J. Müller, E. Silva, A. Alabastri, S. W. Bishnoi, P. Nordlander, N. J. Halas, *ACS Energy Lett.* **2017**, *2*, 8.

[11]   Y. Yang, X. Yang, L. Fu, M. Zou, A. Cao, Y. P. Du, Q. Yuan, C. H. Yan, *ACS Energy Lett.* **2018**, DOI 10.1021/acsenergylett.8b00433.

[12]   Y. Pang, J. Zhang, R. Ma, Z. Qu, E. Lee, T. Luo, *ACS Energy Lett.* **2020**, *5*, 437.

[13]   V. Siva Reddy, S. C. Kaushik, K. R. Ranjan, S. K. Tyagi, *Renew. Sustain. Energy Rev.* **2013**, *27*, 258.

[14]   C. M, A. Yadav, *Renew. Sustain. Energy Rev.* **2017**, *67*, 1308.

[15]   F. Gong, W. Wang, H. Li, D. (David) Xia, Q. Dai, X. Wu, M. Wang, J. Li, D. V. Papavassiliou, R. Xiao, *Appl. Energy* **2020**, *261*, 114410.

[16]   J. Li, X. Zhou, P. Mu, F. Wang, H. Sun, Z. Zhu, J. Zhang, W. Li, A. Li, *ACS Appl. Mater. Interfaces* **2020**, *12*, 798.

[17]   F. Jia, Q. Wang, J. Wu, Y. Li, S. Song, *ACS Sustain. Chem. Eng.* **2017**, *5*, 7410.

[18]   Q. Wang, L. Yang, F. Jia, Y. Li, S. Song, *J. Mol. Liq.* **2018**, *263*, 526.

[19]   Y. Oren, *Desalination* **2008**, *228*, 10.

[20]   G. Amy, N. Ghaffour, Z. Li, L. Francis, R. V. Linares, T. Missimer, S. Lattemann, *Desalination* **2017**, *401*, 16.

[21]   W. Suwaileh, D. Johnson, S. Khodabakhshi, N. Hilal, *Desalination* **2019**, *463*, 1.

[22]   G. Amy, N. Ghaffour, Z. Li, L. Francis, R. V. Linares, T. Missimer, S. Lattemann, *Desalination* **2017**, *401*, 16.

[23]   K. Yu, P. Shao, P. Meng, T. Chen, J. Lei, X. Yu, R. He, F. Yang, W. Zhu, T. Duan, *J. Hazard. Mater.* **2020**, *392*, 122350.

[24]   F. Jiang, H. Liu, Y. Li, Y. Kuang, X. Xu, C. Chen, H. Huang, C. Jia, X. Zhao, E. Hitz, Y. Zhou, R. Yang, L. Cui, L. Hu, *ACS Appl. Mater. Interfaces* **2018**, *10*, 1104.

[25]   C. Liu, J. Huang, C.-E. Hsiung, Y. Tian, J. Wang, Y. Han, A. Fratalocchi, *Adv. Sustain. Syst.* **2017**, *1*, 1600013.

[26]   H. Ghasemi, G. Ni, A. M. Marconnet, J. Loomis, S. Yerci, N. Miljkovic, G. Chen, *Nat. Commun.* **2014**, *5*, 4449.

[27]   S. Hong, Y. Shi, R. Li, C. Zhang, Y. Jin, P. Wang, *ACS Appl. Mater. Interfaces* **2018**, *10*, 28517.

[28]   X. Yin, Y. Zhang, Q. Guo, X. Cai, J. Xiao, Z. Ding, J. Yang, *ACS Appl. Mater. Interfaces* **2018**, *10*, 10998.

[29]   P. Sun, W. Zhang, I. Zada, Y. Zhang, J. Gu, Q. Liu, H. Su, D. Pantelić, B. Jelenković, D. Zhang, *ACS Appl. Mater. Interfaces* **2020**, *12*, 2171.

[30]   J. Wang, Y. Li, L. Deng, N. Wei, Y. Weng, S. Dong, D. Qi, J. Qiu, X. Chen, T. Wu, *Adv. Mater.* **2017**, *29*, 1.

[31]   F. Liu, W. Liang, C. Wang, C. Xiao, J. He, G. Zhao, Z. Zhu, H. Sun, A. Li, *Mater. Today Energy* **2020**, *16*, 100375.

[32]   K. Yu, P. Shao, P. Meng, T. Chen, J. Lei, X. Yu, R. He, F. Yang, W. Zhu, T. Duan, *J. Hazard. Mater.* **2020**, *392*, 122350.

[33]   J. Wang, Y. Li, L. Deng, N. Wei, Y. Weng, S. Dong, D. Qi, J. Qiu, X. Chen, T. Wu, *Adv. Mater.* **2017**, *29*, 1603730.

[34]   F. S. Awad, H. D. Kiriarachchi, K. M. AbouZeid, Ü. Özgür, M. S. El-Shall, *ACS*

Appl. Energy Mater. **2018**, *1*, 976.

[35]   H. Liu, X. Zhang, Z. Hong, Z. Pu, Q. Yao, J. Shi, G. Yang, B. Mi, B. Yang, X. Liu, H. Jiang, X. Hu, *Nano Energy* **2017**, *42*, 115.

[36]   L. Zhang, L. Mu, Q. Zhou, X. Hu, *Water Res.* **2020**, DOI 10.1016/j.watres.2019.115367.

[37]   Z. Guo, Z. Chen, Z. Shi, J. Qian, J. Li, T. Mei, J. Wang, X. Wang, P. Shen, *Sol. Energy Mater. Sol. Cells* **2020**, DOI 10.1016/j.solmat.2019.110227.

[38]   X. Zhang, G. Wu, X.-C. Yang, *ACS Appl. Nano Mater.* **2020**, acsanm.0c01712.

[39]   L. Wang, C. Liu, H. Wang, Y. Xu, S. Ma, Y. Zhuang, W. Xu, W. Cui, H. Yang, *ACS Appl. Mater. Interfaces* **2020**, *12*, 24328.

[40]   N. Ma, Q. Fu, Y. Hong, X. Hao, X. Wang, J. Ju, J. Sun, *ACS Appl. Mater. Interfaces* **2020**, *12*, 18165.

[41]   T. Chen, Z. Wu, Z. Liu, J. T. Aladejana, X. (Alice) Wang, M. Niu, Q. Wei, Y. Xie, *ACS Appl. Mater. Interfaces* **2020**, *12*, 19511.

[42]   Q. Fang, T. Li, H. Lin, R. Jiang, F. Liu, *ACS Appl. Energy Mater.* **2019**, *2*, 4354.

[43]   K.-K. Liu, Q. Jiang, S. Tadepalli, R. Raliya, P. Biswas, R. R. Naik, S. Singamaneni, *ACS Appl. Mater. Interfaces* **2017**, *9*, 7675.

[44]   L. Guo, J. Gong, C. Song, Y. Zhao, B. Tan, Q. Zhao, S. Jin, *ACS Energy Lett.* **2020**, *5*, 1300.

[45]   D. Ghim, Q. Jiang, S. S. Cao, S. Singamaneni, Y. S. Jun, *Nano Energy* **2018**, DOI 10.1016/j.nanoen.2018.09.038.

[46]   E.-D. Miao, M.-Q. Ye, C.-L. Guo, L. Liang, Q. Liu, Z.-H. Rao, *Appl. Therm. Eng.* **2019**, *149*, 1255.

[47]   X. Wang, Y. He, X. Liu, J. Zhu, *Powder Technol.* **2017**, *321*, 276.

[48]   L. Zhu, M. Gao, C. K. N. Peh, X. Wang, G. W. Ho, *Adv. Energy Mater.* **2018**, *8*, 1702149.

[49]   S. Liu, C. Huang, Q. Huang, F. Wang, C. Guo, *J. Mater. Chem. A* **2019**, *7*, 17954.

[50]   G. Wang, Y. Fu, A. Guo, T. Mei, J. Wang, J. Li, X. Wang, *Chem. Mater.* **2017**, *29*, 5629.

[51]   W. Fang, L. Zhao, X. He, H. Chen, W. Li, X. Zeng, X. Chen, Y. Shen, W. Zhang, *Renew. Energy* **2020**, DOI 10.1016/j.renene.2019.11.111.

[52] Z. Tahir, S. Kim, F. Ullah, S. Lee, J. Lee, N.-W. Park, M.-J. Seong, S.-K. Lee, T.-S. Ju, S. Park, J.-S. Bae, J. I. Jang, Y. S. Kim, *ACS Appl. Mater. Interfaces* **2020**, *12*, 2490.

[53] K. Wang, B. Huo, F. Liu, Y. Zheng, M. Zhang, L. Cui, J. Liu, *Desalination* **2020**, *481*, 114303.

[54] M. W. Higgins, A. R. Shakeel Rahmaan, R. R. Devarapalli, M. V. Shelke, N. Jha, *Sol. Energy* **2018**, DOI 10.1016/j.solener.2017.11.055.

[55] J. Tian, X. Huang, W. Wu, *Ind. Eng. Chem. Res.* **2020**, *59*, 1135.

[56] K. K. Liu, Q. Jiang, S. Tadepalli, R. Raliya, P. Biswas, R. R. Naik, S. Singamaneni, *ACS Appl. Mater. Interfaces* **2017**, *9*, 7675.

[57] Z. Hong, J. Pei, Y. Wang, B. Cao, M. Mao, H. Liu, H. Jiang, Q. An, X. Liu, X. Hu, *Energy Convers. Manag.* **2019**, *199*, 112019.

[58] P. Sun, W. Wang, W. Zhang, S. Zhang, J. Gu, L. Yang, D. Pantelić, B. Jelenković, D. Zhang, *ACS Appl. Mater. Interfaces* **2020**, *12*, 34837.

[59] X. Wang, Y. He, X. Liu, G. Cheng, J. Zhu, *Appl. Energy* **2017**, DOI 10.1016/j.apenergy.2017.03.080.

[60] J. Zhou, Y. Gu, Z. Deng, L. Miao, H. Su, P. Wang, J. Shi, *Sustain. Mater. Technol.* **2019**, DOI 10.1016/j.susmat.2018.e00090.

[61] Z. Zheng, H. Li, X. Zhang, H. Jiang, X. Geng, S. Li, H. Tu, X. Cheng, P. Yang, Y. Wan, *Nano Energy* **2020**, DOI 10.1016/j.nanoen.2019.104298.

[62] C. Sheng, N. Yang, Y. Yan, X. Shen, C. Jin, Z. Wang, Q. Sun, *Appl. Therm. Eng.* **2020**, DOI 10.1016/j.applthermaleng.2019.114712.

[63] B. Huo, D. Jiang, X. Cao, H. Liang, Z. Liu, C. Li, J. Liu, *Carbon N. Y.* **2019**, *142*, 13.

[64] Y. Fu, G. Wang, X. Ming, X. Liu, B. Hou, T. Mei, J. Li, J. Wang, X. Wang, *Carbon N. Y.* **2018**, *130*, 250.

[65] S. Tian, Z. Huang, J. Tan, X. Cui, Y. Xiao, Y. Wan, X. Li, Q. Zhao, S. Li, C.-S. Lee, *ACS Energy Lett.* **2020**, *5*, 2698.

[66] H. Wang, A. Du, X. Ji, C. Zhang, B. Zhou, Z. Zhang, J. Shen, *ACS Appl. Mater. Interfaces* **2019**, *11*, 42057.

[67] H. Cheng, X. Liu, L. Zhang, B. Hou, F. Yu, Z. X. Shi, X. Wang, *Sol. Energy Mater.*

Sol. Cells **2019**, DOI 10.1016/j.solmat.2019.110127.

[68]   K. S. Creely, G. W. Hughson, J. Cocker, K. Jones, *Ann. Occup. Hyg.* **2006**, *50,* 609.

[69]   J. E. Lockey, C. A. Redlich, R. Streicher, A. Pfahles-Hutchens, P. (Bert) J. Hakkinen, G. L. Ellison, P. Harber, M. Utell, J. Holland, A. Comai, M. White, *J. Occup. Environ. Med.* **2015**, *57*, 44.

[70]   M. M. Ghafurian, H. Niazmand, E. Ebrahimnia-Bajestan, R. A. Taylor, *Renew. Energy* **2020**, DOI 10.1016/j.renene.2019.08.036.

[71]   F. He, M. Han, J. Zhang, Z. Wang, X. Wu, Y. Zhou, L. Jiang, S. Peng, Y. Li, *Nano Energy* **2020**, DOI 10.1016/j.nanoen.2020.104650.

[72]   Z. Li, M. Zheng, N. Wei, Y. Lin, W. Chu, R. Xu, H. Wang, J. Tian, H. Cui, *Sol. Energy Mater. Sol. Cells* **2020**, DOI 10.1016/j.solmat.2019.110254.

[73]   Z. Yu, S. Cheng, C. Li, Y. Sun, B. Li, *Sol. Energy* **2019**, DOI 10.1016/j.solener.2019.09.080.

[74]   M. Aziznezhad, E. Goharshadi, M. Namayandeh-Jorabchi, *Sol. Energy Mater. Sol. Cells* **2020**, DOI 10.1016/j.solmat.2020.110515.

[75]   L. Su, Y. Hu, Z. Ma, L. Miao, J. Zhou, Y. Ning, Z. Chang, B. Wu, M. Cao, R. Xia, J. Qian, *Sol. Energy Mater. Sol. Cells* **2020**, DOI 10.1016/j.solmat.2020.110484.

[76]   Z. Liu, Y. Pan, K. Shi, W. Wang, C. Peng, W. Li, D. Sha, Z. Wang, X. Ji, *Carbohydr. Polym.* **2016**, DOI 10.1016/j.carbpol.2016.04.004.

[77]   S. Bera, K. Mohanty, *J. Water Process Eng.* **2020**, DOI 10.1016/j.jwpe.2019.100999.

[78]   M. S. Sreekala, J. George, M. G. Kumaran, S. Thomas, *J. Polym. Sci. Part B Polym. Phys.* **2001**, *39,* 1215.

[79]   S. Lai, J. Gao, H. Zhang, L. Cheng, X. Xiong, *J. CO2 Util.* **2020**, DOI 10.1016/j.jcou.2020.01.004.

[80]   S. Yin, H. Wang, J. Li, R. O. Ritchie, J. Xu, *J. Mech. Behav. Biomed. Mater.* **2019**, DOI 10.1016/j.jmbbm.2019.02.029.

[81]   X. Gu, C.-J. Tong, S. Rehman, L.-M. Liu, Y. Hou, S. Zhang, *ACS Appl. Mater. Interfaces* **2016**, *8*, 15991.

[82]   Y. Guo, L. Cao, C. Chen, Y. Lu, R. Luo, Q. Yu, Y. Zhang, Y. Wang, X. Liu, Y. Luo,

ChemistrySelect **2018**, *3*, 5883.

[83] T. Al-Mobarak, M. Mina, M. Gafur, *J. Thermoplast. Compos. Mater.* **2019**, *32*, 967.

[84] D. Yadav, P. Azad, R. Vaish, *Glob. Challenges* **2020**, *4*, 1900080.

[85] Z. Yuan, J. Huang, C. Peng, M. Wang, X. Wang, J. Bin, S. Xing, J. Xiao, J. Zeng, X. Xiao, X. Fu, H. Gong, D. Zhao, H. Chen, *Appl. Phys. A* **2016**, *122*, 125.

[86] M. Zhu, Y. Li, F. Chen, X. Zhu, J. Dai, Y. Li, Z. Yang, X. Yan, J. Song, Y. Wang, E. Hitz, W. Luo, M. Lu, B. Yang, L. Hu, *Adv. Energy Mater.* **2018**, *8*, 1701028.

[87] G. Xue, K. Liu, Q. Chen, P. Yang, J. Li, T. Ding, J. Duan, B. Qi, J. Zhou, *ACS Appl. Mater. Interfaces* **2017**, *9*, 15052.

[88] Y. Bian, Q. Du, K. Tang, Y. Shen, L. Hao, D. Zhou, X. Wang, Z. Xu, H. Zhang, L. Zhao, S. Zhu, J. Ye, H. Lu, Y. Yang, R. Zhang, Y. Zheng, S. Gu, *Adv. Mater. Technol.* **2019**, *4*, 1800593.

[89] H. Ghasemi, G. Ni, A. M. Marconnet, J. Loomis, S. Yerci, N. Miljkovic, G. Chen, *Nat. Commun.* **2014**, *5*, 4449.

[90] B. Li, L. Li, L. Wu, J. Zhang, A. Wang, *Chempluschem* **2014**, *79*, 850.

[91] C. Jia, Y. Li, Z. Yang, G. Chen, Y. Yao, F. Jiang, Y. Kuang, G. Pastel, H. Xie, B. Yang, S. Das, L. Hu, *Joule* **2017**, *1*, 588.

[92] T. A. Cooper, S. H. Zandavi, G. W. Ni, Y. Tsurimaki, Y. Huang, S. V Boriskina, G. Chen, *Nat. Commun.* **2018**, *9*, 5086.

[93] Y. Chen, Y. Shi, H. Kou, D. Liu, Y. Huang, Z. Chen, B. Zhang, *ACS Sustain. Chem. Eng.* **2019**, *7*, 2911.

[94] C. Chen, Y. Li, J. Song, Z. Yang, Y. Kuang, E. Hitz, C. Jia, A. Gong, F. Jiang, J. Y. Zhu, B. Yang, J. Xie, L. Hu, *Adv. Mater.* **2017**, *29*, 1701756.

[95] X. Gao, H. Lan, S. Li, X. Lu, M. Zeng, X. Gao, Q. Wang, G. Zhou, J.-M. Liu, M. J. Naughton, K. Kempa, J. Gao, *Glob. Challenges* **2018**, *2*, 1800035.

[96] S. Liu, C. Huang, X. Luo, C. Guo, *Appl. Energy* **2019**, *239*, 504.

[97] T. Karthik, P. Ganesan, *J. Text. Inst.* **2016**, *107*, 1412.

[98] P. Daniel, *Int. J. Sci. Res. Manag.* **2016**, 4514.

[99] Y.-Y. Ma, C.-X. Wu, X.-J. Feng, H.-Q. Tan, L.-K. Yan, Y. Liu, Z.-H. Kang, E.-B. Wang, Y.-G. Li, *Energy Environ. Sci.* **2017**, *10*, 788.

[100] H. Galal-Gorchev, *Water Supply* **1993**, *11*, 1.

[101] World Health Organization, *Tech. Notes Drink. Sanit. Hyg. Emergencies.* **2013**, 1.